Deposition potential of 0.003-10 mu m ambient particles in the humidified human respiratory tract : Contribution of new particle formation events in Beijing

Ma, Li

2022-09-15

Ma , L , Zhang , Y , Lin , Z , Zhou , Y , Yan , C , Zhang , Y , Zhou , W , Ma , W , Hua , C , Li , X , Deng , C , Qi , Y , Dada , L , Li , H , Bianchi , F , Petäjä , T , Kangasluoma , J , Jiang , J , Liu , S , Hussein , T , Kulmala , M & Liu , Y 2022 , ' Deposition potential of 0.003-10 mu m ambient particles in the humidified human respiratory tract : Contribution of new particle formation events in Beijing ' , Ecotoxicology and Environmental Safety , vol. 243 , 114023 . https://doi.org/10.1016/j.e

Deposition potential of 0.003–10 μm ambient particles in the humidified human respiratory tract: Contribution of new particle formation events in Beijing

Li Ma [a], Ying Zhang [a], Zhuohui Lin [a], Ying Zhou [a], Chao Yan [b], Yusheng Zhang [a], Wenshuo Zhou [a], Wei Ma [a], Chenjie Hua [a], Xiaoxiao Li [c], Chenjuan Deng [c], Yu Qi [d], Lubna Dada [b], Hongyan Li [e], Federico Bianchi [b], Tuukka Petäjä [b], Juha Kangasluoma [a,b], Jingkun Jiang [c], Sijin Liu [d], Tareq Hussein [b,f], Markku Kulmala [a,b], Yongchun Liu [a,*]

[a] *Aerosol and Haze Laboratory, Advanced Innovation Center for Soft Matter Science and Engineering, Beijing University of Chemical Technology, Beijing 100029, China*
[b] *Institute for Atmospheric and Earth System Research/Physics, Faculty of Science, University of Helsinki, Finland*
[c] *State Key Joint Laboratory of Environment Simulation and Pollution Control, School of Environment, Tsinghua University, 100084 Beijing, China*
[d] *State Key Laboratory of Environmental Chemistry and Ecotoxicology, Research Center for Eco-Environmental Sciences, Chinese Academy of Sciences, Beijing 100085, China*
[e] *School of Environment and Safety, Taiyuan University of Science and Technology, Taiyuan, Shanxi, 030024, China*
[f] *The University of Jordan, Department of Physics, Amman 11942, Jordan*

ARTICLE INFO

ABSTRACT

Ultrafine particles (UFPs) usually explosive growth during new particle formation (NPF) events. However, the risk of exposure to UFPs on NPF days has been ignored due to the prevalence of mass-based air quality standards. In this study, the daily deposited doses, i.e., the daily deposited particle number dose (D_{PNd}), mass dose (D_{PMd}), and surface area dose (D_{PSd}), of ambient particles in the human respiratory tract in Beijing were evaluated based on the particle number size distribution (3 nm-10 μm) from June 2018 to May 2019 utilizing a Multiple-Path Particle Dosimetry Model (MPPD) after the hygroscopic growth of particles in the respiratory tract had been accounted for. Our observations showed a high frequency (72.6%) of NPF on excellent air quality days, with daily mean PM$_{2.5}$ concentrations less than 35 μg m^{-3}. The daily D_{PNd} on excellent air quality days was comparable with that on polluted days, although the D_{PMd} on excellent air quality days was as low as 15.6% of that on polluted days. The D_{PNd} on NPF days was ~1.3 times that on non-NPF days. The D_{PNd} in respiratory tract regions decreased in the order: tracheobronchial (TB) > pulmonary (PUL) > extrathoracic (ET) on NPF days, while it was PUL > TB > ET on non-NPF days. The number of deposited nucleation mode particles, which were deposited mainly in the TB region (45%), was 2 times higher on NPF days than that on non-NPF days. Our results demonstrated that the deposition potential due to UFPs in terms of particle number concentrations is high in Beijing regardless of the aerosol mass concentration. More toxicological studies related to UFPs on NPF days, especially those targeting tracheobronchial and pulmonary impairment, are required in the future.

1. Introduction

Particulate matter (PM) is a complex mixture of inorganic and carbonaceous constituents. It originates from a wide variety of natural and anthropogenic emission sources, such as the incomplete combustion of fossil fuels, biomass burning, volcanic eruptions, sea salt, road and mineral dust, and the oxidation of volatile organic compounds (VOCs) (Almeida et al., 2020). Epidemiological studies have revealed connections between particle exposure and cardiovascular diseases (e.g., thrombogenesis, atheromatous plaques), respiratory diseases (e.g.,

chronic obstructive pulmonary disease (COPD), asthma) (Terzano et al., 2010) and lung cancer (Tie et al., 2009). PM$_{2.5}$ (with aerodynamic diameter < 2.5 μm), which is the main respirable type of PM, was ranked as the fifth mortality risk factor in 2015 and caused more than 4.2 million deaths worldwide (Cohen et al., 2017). A recent study demonstrated a positive correlation between PM$_{2.5}$ pollution and the severity in COVID-19 patients (Paital and Agrawal, 2021). Thus, the health effects of PM have attracted much attention worldwide.

Generally, air quality standards and most particle toxicological studies are based on exposure to particle mass concentrations (PMCs). However, these PMC-based studies might overlook the health impact of ultrafine particles (UFPs, with d_p <100 nm) from combustion sources and new particle formation (NPF) events characterized by high particle number concentrations (PNCs) of UFPs but low PMCs (Morawska et al., 2008). UFPs with high specific surface areas are capable of absorbing more potentially toxic chemical substances (e.g., transition metals, quinones, polycyclic aromatic hydrocarbons) (Sioutas et al., 2005). They can also penetrate the lungs (Lu et al., 2020), the circulatory system (Miller et al., 2017), the heart (Calderon-Garciduenas et al., 2019), and the brain (Oberdorster et al., 2004), and so on. Atmospheric NPF is the dominant source of UFPs in the atmosphere and has attracted much attention in recent years. NPF events usually occur on clean days and are driven by photochemical reactions (Gao et al., 2012; Chu et al., 2021); they are characterized by a sharp increase in UFP concentrations. Our recent study found that over 65% of the number concentration of haze particles resulted from NPF in Beijing (Kulmala et al., 2020). The PMC has declined greatly in China since the central government executed the Air Pollution Prevention and Control Action Plan in 2013 and the measure further reduced PM$_{2.5}$-attributable excess deaths by 0.37 million from 2013 to 2017 (Zhang et al., 2019), meanwhile, Li's research showed national PM$_{2.5}$ related deaths from stroke, ischemic, chronic obstructive pulmonary disease (COPD), lung cancer and acute lower respiratory infection increased from approximately 0.89 million cases in 1998 to the peak of 1.34 million in 2014 and steadily declined to 1.17 million cases in 2017 (Li et al., 2018). The improvement of air quality tends to decrease the condensation sink (CS) but enhance the survivability of UFPs and, subsequently, the frequency of NPF (An et al., 2015). For example, higher NPF event frequencies were observed due to emission reduction associated with special activities, such as the parade in 2015 and the Olympics in 2008 (August 8–23), than in 2010–2013 (Shen et al., 2016). It should be noted that the starting times of NPF events usually overlap with the morning commuting period. Given the abundance of UFPs after nucleation on NPF days and their roles in premature deaths and morbidity (Donaldson et al., 2002), it is necessary to quantitatively evaluate the potential risks of exposure to a high-PNC environment driven by NPF in China. In addition, the particle size on NPF days is different from that on pollution days, suggesting a different health effect of NPF events. However, it has attracted less attention at the present.

It should be noted that only particles deposited in the respiratory tract can interact with bio-molecules and cells, consequently leading to adverse biological effects. This means particle deposited dose should be more closely associated with health outcomes than the ambient concentrations. However, quantitative studies on particle deposition in the human respiratory tract are scarce in Beijing due to the limited availability of size-segregated particle measurements. Only one study utilized the Multiple-Path Particle Dosimetry Model (MPPD) to simulate the deposition of size-segregated particles from 5.6 to 560 nm in the human airway assuming that the particles are hydrophobic (in December 2011 and April 2012) (Li et al., 2016). However, after aerosol particles are inhaled into the respiratory tract, the condensation of water vapor on the particles will lead to particle growth, and subsequently change the deposition efficiency of aerosol particles, as the relative humidity (RH) can be as high as 99.5% in the human respiratory tract (Asgharian, 2004). Thus, the regional deposition behavior might deviate from that predicted by the model if hygroscopic growth in the respiratory tract is

not accounted for (Asgharian, 2004).

In this study, we performed size-segregated particle measurements from 3 nm to 10 μm (aerodynamic diameter, d_a) over one year of observation in downtown Beijing. The deposition potential of UFPs for Chinese adults was evaluated utilizing the MPPD model after the hygroscopic growth of particles in the respiratory tract was considered. The contribution of NPF events to the exposure risks of UFPs was in particular discussed. This work will provide comprehensive insight into the potential health risks from ambient particles in Beijing.

2. Methods

2.1. Field measurements

Observations were carried out at the Aerosol and Haze Laboratory, Beijing University of Chemical Technology (AHL/BUCT) station, which is located at 98 Zizhuyuan Road, Haidian District. Details about the AHL/BUCT station can be found in our previous work (Chu et al., 2021; Liu et al., 2020; Zhou et al., 2020). Briefly, it is on a rooftop of the main building, which is 550 m from the 3rd Ring Road to the east, 130 m from Zizhuyuan Road to the north, and 565 m from Landianchang Road to the west (Fig. S1). The station is surrounded by traffic and residential emissions, representing a typical urban observation station.

Observations were conducted from June 2018 to May 2019. Mass concentration of PM$_{2.5}$ was measured using a TEOM (1405-DF, Thermo Fisher). Following instruments were deployed to obtain a wide range of particle sizes. The distribution of particle sizes from 2 to 40 nm (mobility diameter, d_m) was measured with a Neutral cluster and Air Ion Spectrometer (NAIS, model 4–11). The particles from 6 to 840 nm (d_m) were measured with a Differential Mobility Particle Sizer (DMPS, University of Helsinki), which consisted of a Differential Mobility Analyzer (custom made) and a Condensation Particle Counter (CPC 3772, TSI). The particles from 550 nm to 10 μm (d_a) were measured by an Aerodynamic Particle Sizer (APS 3321, TSI). Statistics for the missing dataset during our observation are shown in Table S1. A Particle Size Distribution (PSD) measuring device, which consisted of a nano-DMA (3085, TSI), a long DMA (3081, TSI) coupled with a CPC (3776, TSI), and an APS, was used to measure the particles from 3 to 10,000 nm. However, this device was only available from November to December 2018.

2.2. Data pre-processing

The particle size distribution collected by the NAIS was determined using the correction factor (CF) with Eq. (1) when both the PSD and NAIS data were available. The calculated size-dependent CF values are presented in Table S2.

$$CF_i = \frac{n_{PSD,i}}{n_{NAIS,i}} \tag{1}$$

where $n_{PSD,i}$ and $n_{NAIS,i}$ are the number concentration of particles with mobility diameter (d_m) values of i nm measured by the PSD and NAIS, respectively.

The NAIS and DMPS measure the electrical mobility diameter (d_m) of particles. We converted the particle d_m into d_a according to Eq. (2). Like in other studies, both the shape factor and the C_c were assumed to be 1.0 (Li et al., 2016). The particle mass concentration (μg m^{-3}) and particle surface concentration (PSC, μm^2 cm^{-3}) were further calculated based on Eqs. (3, 4).

$$d_a = d_m \sqrt{x \times \frac{\rho \times C_{c(d_m)}}{C_{c(d_a)}}} \tag{2}$$

$$MC_i = \left(\frac{\pi}{6}\right) \cdot d_a^3 \cdot \rho \cdot NC_i \cdot 10^{-9} \tag{3}$$

$$SC_i = 4\pi d_a^2 \cdot NC_i \cdot 10^{-6} \tag{4}$$

where d_a is the aerodynamic diameter (nm), d_m is the mobility diameter (nm), and ρ is the particle density which showed seasonal and diurnal variations, with higher values during the warm season (1.60 ± 0.43 g cm^{-3}, July to September 2014) compared to the cold season (1.41 ± 0.40 g cm^{-3}, November 2013 to January 2014) (Liu et al., 2015). We assumed a mean particle density is 1.5 g cm^{-3} based on a previous study in Beijing (Hu et al., 2012), χ is the shape factor, C_c is the Cunningham slip correction factor for a certain diameter, and NC_i, MC_i, and SC_i represent the number, mass and surface concentration of particles in the ith bin with the cut-off diameter.

The particle size spectra from 3 nm to 10 μm (d_a) was merged using the corrected NAIS data for 2–20 nm (d_m, i.e., 3–30 nm in d_a), the DMPS data for 20–453 nm (d_m, i.e., 30–679.5 nm in d_a), and the APS data for 523 nm-10 μm (d_a). The moving average method, which creating a series of averages of different subsets of the full data set to smooth the dataset in the overlapping ranges, was used to process the merged data.

2.3. Particle deposition in the respiratory tract

The International Commission on Radiological Protection (ICRP) and the Multiple-Path Particle Dosimetry Model (MPPD) models are the most popular computational models for predicting particle deposition in the whole and regional airways, including the extrathoracic (ET), tracheobronchial (TB) and pulmonary (PUL) regions. The ICRP model is a semi-empirical model that determines the deposition fraction of particles in airway regions based on numerical fitting experimental data and theoretical calculations. The MPPD model developed by Applied Research Associates, Inc. and the Hamner Institutes for Health Sciences is the most realistic deposition model and considers the branching asymmetry of airways based on detailed lung geometries. The regional deposition fractions predicted by the ICPR and MPPD models for a Chinese human in a resting state are shown in Fig. S2. Both models show U-shaped total deposition curves. The ICPR model likely overestimates the total deposition efficiency in the PUL region but underestimates it in the TB region for particles with diameters less than 100 nm. For particles larger than 100 nm, the discrepancy between those two models is small.

In this study, we applied the MPPD model (version 3.04) to quantify aerosol deposition in the respiratory system because we are interested in the contribution of new particle formation events, which are dominated by small particles (d_p<100 nm), to the deposition potential of ambient particles in the human respiratory tract. Detailed descriptions of the model can be found elsewhere (Manojkumar et al., 2019). Briefly, this model can calculate the deposition fraction (DF) of particles after incorporating the exposure concentration of particles, parameters associated with respiration functional residual capacity (FRC), upper respiratory tract volume (URTV), breathing frequency (BF), tidal volume (TV) and health status of the specific population. A stochastic lung model (lung size-total 60th percentile of the airway) was used to calculate the DF of particles in the airways of Chinese adults. The relevant respiration parameters, including FRC, URTV, BF, and TV, were 2950 mL, 44.7 mL, 16 min^{-1}, and 537.5 mL, respectively (Roy et al., 1991). The default values of the model were used for the rest parameters. The details for the parameters are provided in Table S3.

Many factors, such as age, gender, activity, and health status, also influence the deposition efficiency simulation. For example, Manojkumar found that 8-year-old children had the maximum size-segregated PM deposition, while 28-month-old infant groups experienced the minimum PM deposition (Manojkumar et al., 2019). The deposition dose during exercise could be 4.5 times that in a resting state (Daigle et al., 2003). Patients with COPD or asthma are subject to increased exposure to UFPs compared with healthy persons (Chalupa et al., 2004). However, in this study, we focused on only the average respiratory characteristics of healthy Chinese adults.

Condensation of water vapor at high RH (99.5%) leads to particle growth in the human airway. This means the actual deposition curves are different from that predicted with the size distribution of dry particles in the ambient air. Thus, additional corrections were performed for the size distribution of the inhaled particles according to the hygroscopic growth factor (G_f), which is defined as the diameter ratio of wet particles to dry particles, namely $d_{p,wet}/d_{p,dry}$. Ambient aerosols have been classified into three groups by G_f value, e.g., nearly hydrophobic (NH, G_f =1.01–1.14), less hygroscopic (LH, G_f~1.14–1.32), and more hygroscopic (MH, G_f =1.34–1.63) (Vu et al., 2015). According to the measured size-dependent G_f (d_p from 30 to 350 nm) at 90% RH for these three groups of aerosols in urban Beijing (Massling et al., 2009) (Table S4), we interpolated the G_f values in the same size range and extrapolated that out of the size ranges (3–30 nm and 350 nm – 10 μm) according to the best fitted-curves (Fig. S3). Then, the corresponding G_f values in the lungs (99.5% RH) were calculated according to the following equations (Vu et al., 2015),

$$G_f = \sqrt[3]{1 + \kappa_R \cdot \frac{M_w}{\rho_w} \cdot \left(\frac{a_w}{1 - a_w} \right)} \tag{5}$$

$$a_w = \frac{RH}{100 c_k} \tag{6}$$

$$c_k = \exp\left(\frac{4 M_w \sigma_s}{RT \rho_w Dp} \right) \tag{7}$$

where a_w, M_w and ρ_w are the water activity, molecular weight, and density of water, respectively; κ_R represents the effective number of moles of soluble entities per dry particle volume unit; σ_s is the surface tension of the solution (0.072 J/m^2), R and T are the ideal gas constant and temperature, respectively; and c_k is the Kelvin curvature correction factor.

The size-dependent DF in the airways was calculated with the MPPD model using the growth corrected particle size at 99.5% RH as the inputs for each type of hygroscopic particle. Finally, the mean DF was calculated according to (Vu et al., 2015),

$$DF = \alpha \cdot DF_{NH} + \beta \cdot DF_{LH} + \gamma \cdot DF_{MH} \tag{8}$$

where, DF_{NH}, DF_{LH}, DF_{MH} are deposition fractions of nearly hydrophobic particles, less-hygroscopic particles, and more hygroscopic particles, respectively. α, β, γ ($\alpha + \beta + \gamma = 1$) are the number fractions of NH, LH, and MH particles, respectively. The number fractions out of the ranges of 30–350 nm were assumed to be equal to the corresponding boundary values at 30 and 350 nm, respectively (Hussein et al., 2013).

2.4. A Calculation of daily deposited dose

The daily deposited particle number dose (D_{PNd}, particles day^{-1}), deposited mass dose (D_{PMd}, μg day^{-1}), and deposited surface dose (D_{PSd}, cm^2 day^{-1}) were calculated according to Eqs. (9–11),

$$D_{PNd} = \sum_{j=1}^{n} NC_j \cdot VE \cdot DF_{i,j} \cdot t_j \tag{9}$$

$$D_{PMd} = \sum_{j=1}^{n} MC_j \cdot VE \cdot DF_{i,j} \cdot t_j \tag{10}$$

$$D_{PSd} = \sum_{j=1}^{n} SC_j \cdot VE \cdot DF_{i,j} \cdot t_j \tag{11}$$

where NC_j, MC_j, and SC_j are the total number, mass, and surface area concentration. $DF_{i,j}$, and t final deposition fraction and exposure time of particles ($\sum_{j=1}^{n} t_j = 24$ hours), respectively; VE is the minute ventilation ($VE=BF \cdot TV$, 0.516 m^3 h^{-1}).

3. Results and discussion

3.1. Effects of hygroscopic growth on deposition efficiency of particles

Similar to previous studies, a valley-shaped deposition curve of particles is shown in the ET region if the hygroscopic growth has not been considered (Fig. 1A). The deposition is dominated by diffusion of nanometer particles when the d_p is less than 10 nm, while it is mainly contributed by impaction and sedimentation for large particles (Asgharian, 2004). A peaked deposition efficiency presents at ~6 nm in the TB region, followed by a terrace for particles over ~100 nm. A bimodal deposition curve is shown in the PUL region, with the first and the second peak at around 20 nm and 1.2 μm. Thus, the total deposition is a U-shape curve as shown in Fig. 1D.

After hygroscopic growth is accounted for, the *DF* curves in different regions of the lung show the same shapes as their counterparts as shown in Fig. 1. However, all the deposition curves essentially shift to the left side when the aerosol hygroscopicity is taken into consideration. When the d_p is less than 10 nm, hygroscopic growth is negligible. Thus, the deposition curves in all the regions of the respiratory tract coincide well regardless of the particle hygroscopicity. The offset becomes prominent in the large size region driven by the growth of particles in the airways (Fig. S3). Hygroscopic particles with a larger diameter (Dp>200 nm) showed higher total deposition than hydrophobic particles. This indicates an increased deposition fraction for large particles in the human airways. This can be well explained by the fact that the growth factor (*GF*) of particles greatly depends on particle size, i.e., the smaller particle size, the smaller *GF*, due to the Kelvin effect of small particles (Sjogren et al., 2007). Large particles thus tend to grow to larger particles, and then deposit in the airways via impaction and sedimentation. In the following sections, we calculate the deposition doses of particles based on the deposition curves after correcting the hygroscopic growth in the respiratory tract.

3.2. Overview of the dataset and classification of events

Fig. 2 shows the time series of the daily averaged particle number size distribution (PNSD) and depositable PNSD (dPNSD) in the airway during our observations. The x-axis represents time, and the y-axis and the color bar show the particle diameter and the particle number concentration, respectively, on a logarithmic scale. The highest PNC and depositable PNC (dPNC) occurred in December, and the dPNC in the airway decreased in the order: PUL > TB > ET. The statistical parameters for the size-segregated PNC in different modes are summarized in Table S5. The mean concentrations of the particles in nucleation mode (Nuc., 3–25 nm), Aitken mode (Ait., 25–100 nm), accumulation mode (Acc.,100–1000 nm), and coarse mode ($d_a > 1$ μm) (Zhou et al., 2020) were 5947 ± 5559 cm^{-3}, 9433 ± 4683 cm^{-3}, 3768 ± 2759 cm^{-3}, and 4 ± 12 cm^{-3}, respectively. These values were lower than those observed in a two-year observation conducted in Beijing in March 2004 (with corresponding values of 9000 cm^{-3}, 15,900 cm^{-3}, 7800 cm^{-3}, and <1 cm^{-3}) (Wu et al., 2008). The total dPNC (8264 cm^{-3}), which accounting for 43% of the total PNC (19,152 cm^{-3}), had a similar diurnal variation of the total PNC (Fig. S4).

To understand the differences in particle exposure risk between NPF and non-NPF days, the dataset was classified into two groups according to the protocol proposed by Maso et al. (2005). Briefly, a day was identified as an NPF day if particles burst in nucleation mode, followed by growth within several hours; otherwise, the day was classified as a "non-NPF" day. We also classified the annual data into five air quality groups, excellent days (e), good days (g), slightly polluted days (sp), moderately polluted days (mp), and heavily polluted days (hp), according to the daily mean PM$_{2.5}$ mass concentration (Ji et al., 2016). The sp, mp, hp were collectively called polluted days. The daily details about the NPF events and pollution levels during our observations are shown on a calendar (Fig. S5) and in Table S6. There were 294 days with reliable data during our observation periods. The numbers of excellent,
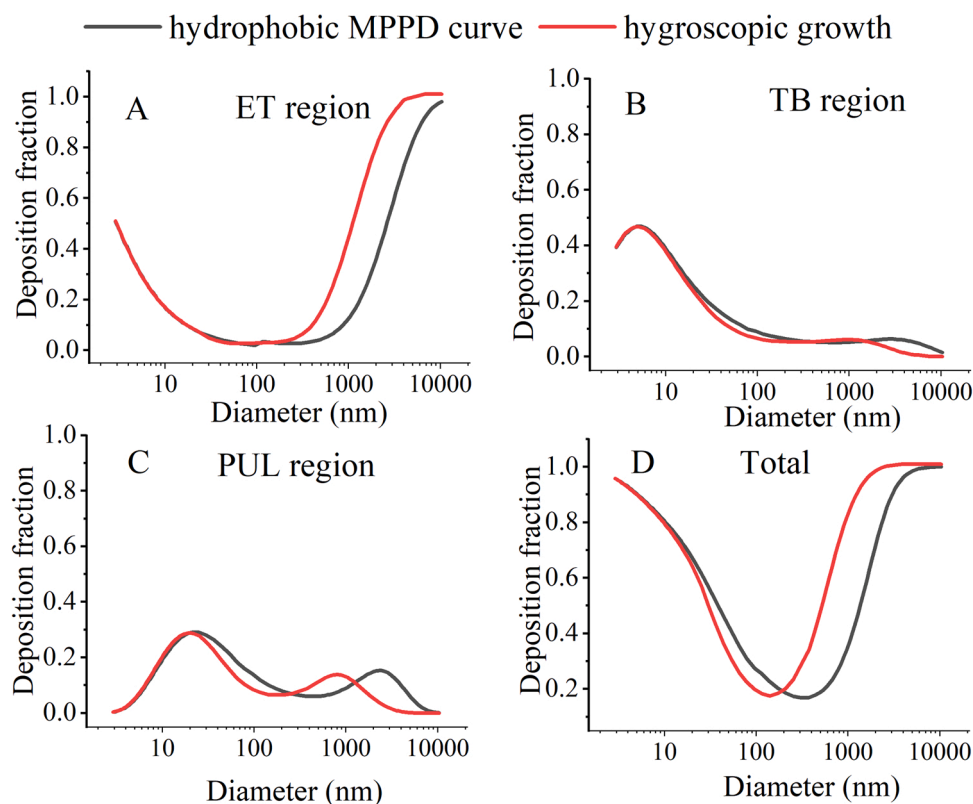

Fig. 1. Comparison the deposition fractions of particles in different regions of the respiratory tract with hydrophobic MPPD curve and with considering hygroscopic growth.
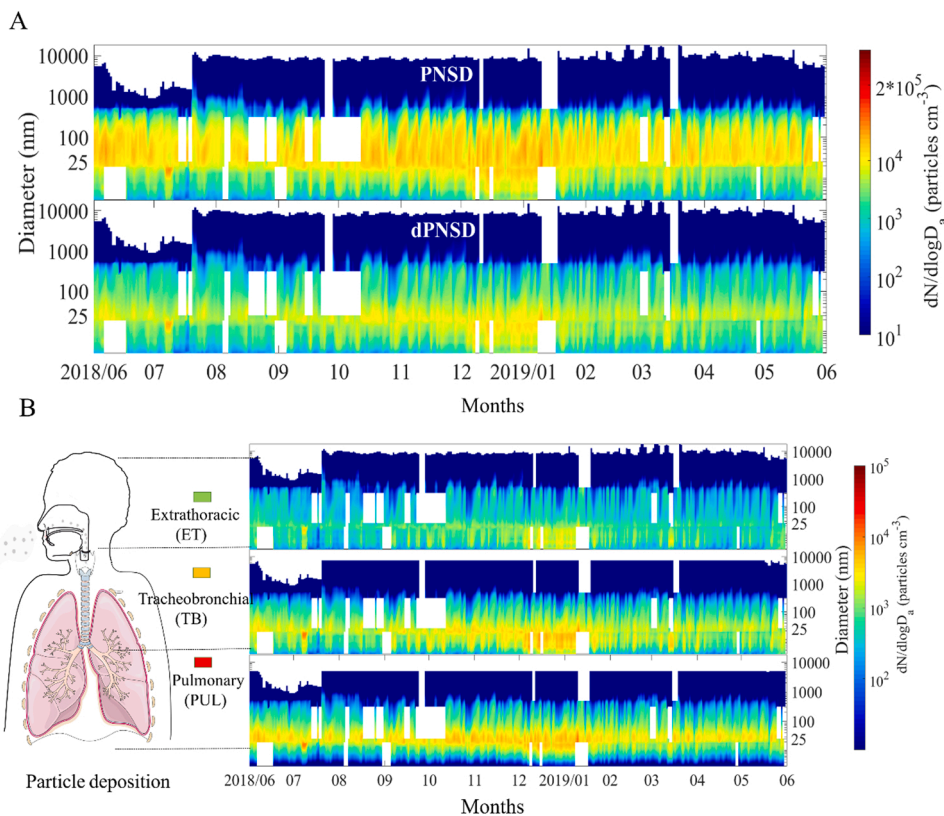
Fig. 2. The annual pattern of the daily averaged particle number size distribution (PNSD) and depositable PNSD (dPNSD) in the airway from June 2018 to May 2019 at the BUCT station. A. PNSD and total dPNSD. B. dPNSD in the ET, TB and PUL regions. These data were measured with NAIS, DMPS and APS in size ranges (d_a) of 3–30 nm, 30–679.5 nm, and 523 nm-10 μm, respectively.
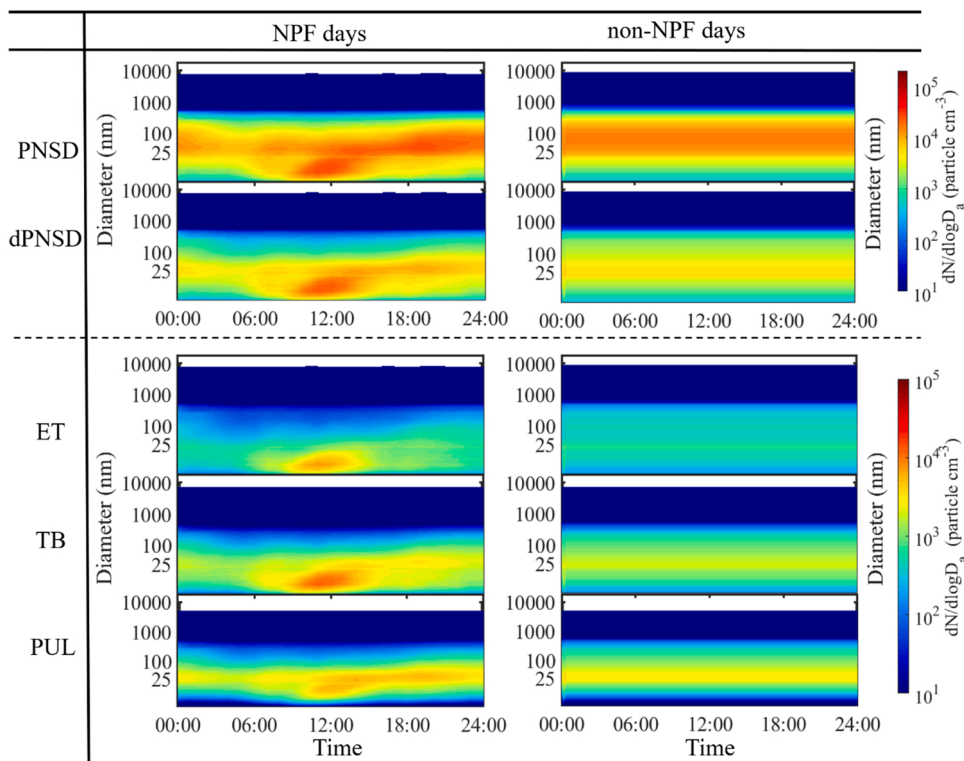

Fig. 3. Diurnal variations of PNSD, dPNSD, and dPNSD in ET, TB, PUL regions on NPF days and non-NPF days. The temporal resolution of every data point in the particle number size distribution is 8 min.

good, slightly polluted, moderately polluted, and heavily polluted days were 146, 103, 28, 9, and 8, respectively, with corresponding frequencies of 49.7%, 35.0%, 9.5%, and 3.1%, and 2.7%. In addition, 128 NPF events out of 294 days were identified throughout the whole year. The annual NPF frequency was 43.5% during our observation period, which was slightly higher than those reported in 2004 (40%) (Wu et al., 2007) and from 2018 to 2019 (30.9%) (Deng et al., 2020) based on a one-year statistical analysis in urban Beijing. NPF events occurred with high frequency (72.6%) on excellent days. On good days and polluted days, the NPF frequencies were 19.4% and 7.1%, respectively. The high NPF frequency in this study might be partially explained by the decrease in condensation sink due to improvement of air quality in the Beijing-Tianjin-Hebei region (BTH) after 2013 (Zhang et al., 2019).

3.3. Particle exposure risk on NPF days and non-NPF days

The diurnal patterns of PNSD and dPNSD on NPF days were different from that on non-NPF days (Fig. 3). On NPF days, the explosive growth of UFPs was observed from 8:00–16:00, with a peak of d_p at less than 50 nm at approximately 12:00–14:00 (Fig. 3). This is consistent with the particle size evolution in a typical NPF event promoted by photochemical processes (Gao et al., 2012). Meanwhile, the explosive growth of UFPs was deposited in ET and TB regions (Fig. 3). However, the corresponding diurnal variations were almost flat on non-NPF days (Fig. 3). The daily D_{PNd} on NPF days (approximately 100.7×10^9 particles day^{-1}) was ~1.3 times great than that on non-NPF days (77.5×10^9 particles day^{-1}) (Table 1). The D_{PNd} in the different airway regions on NPF days was also approximately 1.1–1.6 times that on non-NPF days. Particularly, it is worth noting that the number of deposited nucleation mode particles on NPF days increased 2 times that on non-NPF days, and the majority of those mode particles (45%) deposited in the TB region on NPF days. The sequence of D_{PNd} was TB > PUL > ET on NPF days, while it was PUL > TB > ET on non-NPF days (Fig. 3 and Table 1). These results indicated that TB tended to be influenced by NPF events from the perspective of particle number.

In terms of daily deposited mass (D_{PMd}) and surface area dose (D_{PSd}), they were 162 µg day^{-1} mass and 48 cm^2 day^{-1}, respectively, on NPF days (Table 1). Both of them were much lower than the corresponding value on non-NPF days (475 µg day^{-1} and 130 cm^2 day^{-1}, respectively). Thus, we can conclude that: i) the daily deposited dose based on particle number on NPF days shows a significant increase (100.7×10^9 particles day^{-1}) when compared to that on non-NPF days, which is in contrast with the deposited dose based on particle mass and surface area concentrations and highlights a high inner exposure risk of ultrafine particles (nucleation mode) on NPF days; ii) the TB region of the human respiratory tract should be more easily attacked by ultrafine particles on NPF days in terms of D_{PNd}, whereas the ET region is the target part dominated by accumulation mode particles on both NPF and non-NPF days in terms of D_{PMd} and D_{PSd}. Therefore, the use of a single exposure metric is likely to prove inadequate for eliciting exposure-response functions for all health outcomes. Our results suggest that more attention should be given to UFPs generated during NPF events, which usually occur on excellent days from the perspective of PNC.

3.4. Particle exposure risk at different pollution levels

Fig. 4 compares the diurnal variations of the PNSD and dPNSD at different pollution levels. The temporal variation in the all-day PNSD followed traffic density trends and displayed a three-peak pattern, e.g., in the early morning (08:00), at midday (12:00–13:00), and in the evening (20:00). These peaks were associated with traffic emissions, photochemical production, condensation sinks of UPFs, and the evolution of the mixing layer height (MLH) (Wagner and Schäfer, 2017). The diurnal patterns of PNSD on excellent days and polluted days were quite different. On excellent days, the PNSD had a bimodal distribution that peaked at approximately 10 and 40 nm, respectively, and showed

Table 1
Daily deposited dose based on particle number, particle mass, and particle surface area on NPF days and non-NPF days.

Regions		Particle number dose (×10⁹ particles day⁻¹)					Particle mass dose (µg day⁻¹)					Particle surface dose (cm² day⁻¹)				
		Nucleation	Aitken	ACC	Coarse (×10⁶)	D_{PNd}	Nucleation	Aitken	ACC	Coarse	D_{PMd}	Nucleation	Aitken	ACC	Coarse	D_{PSd}
NPF days	Total	63.3	33.3	4.1	7.3	100.7	0.15	5.63	59.04	97.22	162.04	1.38	12.64	29.72	4.84	48.58
	ET	14.7	3.4	0.8	5.6	18.9	0.02	0.73	15.48	90.24	106.47	0.22	1.50	6.93	4.27	12.92
	TB	28.5	10.8	1.1	0.3	40.4	0.05	1.86	10.17	2.06	14.14	0.54	4.16	6.03	0.14	10.87
	PUL	16.5	16.6	1.3	0.5	34.4	0.06	2.55	15.74	1.93	20.28	0.54	5.94	8.55	0.17	15.2
non-NPF days	Total	31.8	34.2	11.5	21.2	77.5	0.12	7.64	225.52	242.20	475.48	0.99	15.69	101.31	12.57	130.56
	ET	6.2	3.6	2.3	15.9	12.1	0.02	1.04	63.17	222.79	287.02	0.14	1.97	25.18	10.91	38.2
	TB	13.4	11.2	2.8	1.1	27.4	0.04	2.54	35.35	5.48	43.41	0.37	5.19	18.75	0.40	24.71
	PUL	10.5	16.8	3.6	1.7	30.9	0.05	3.39	57.73	5.47	66.64	0.42	7.21	27.94	0.49	36.06

Note: Nucleation mode (3–25 nm), Aitken mode (Ait., 25–100 nm), accumulation mode (Acc., 100–1000 nm), and coarse mode ($d_a > 1$ µm) particles. ET, TB, and PUL represent the Extrathoracic, Tracheobronchial, and Pulmonary regions, respectively.
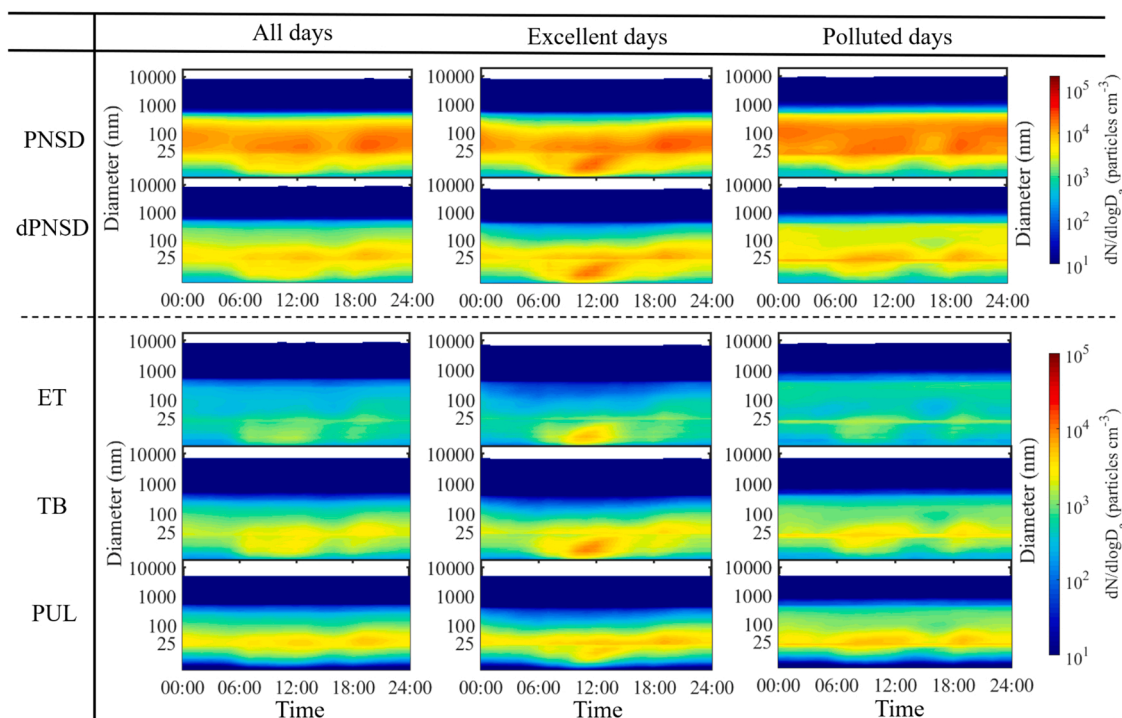
Fig. 4. Diurnal variations of PNSD, dPNSD, and dPNSD in ET, TB, PUL regions at different pollution levels.

obvious particle growth from 3 to ~100 nm starting from 8:00–16:00 accompanied by the observable peak in rush hours (Fig. 4). The growth of particles coincided well with the diurnal variation in photochemical activity (Park et al., 2008). On polluted days, the contribution of accumulation mode particles increased obviously, as evidenced by a shift in the particle size to over 100 nm.

Fig. 4 also shows the diurnal dPNSD in the different airway regions and at different pollution levels. The diurnal patterns of the dPNC in the different airway regions were somewhat similar to the corresponding PNC patterns. For example, the peaks of the dPNC due to vehicular traffic emissions at rush hours were prominent at different pollution levels, and the gradual increase due to NPF events was also observable. However, fewer particles in the middle size range (from 30 to 200 nm) were deposited in the human airway than the corresponding PNC because the particles in the middle size range had a lower deposition fraction than the ultrafine and coarse particles (Fig. 1). Although the deposition fraction curves of particles varied greatly among the ET, TB, and PUL regions (Fig. 1), the diurnal patterns of dPNC among the different airway regions were similar at certain pollution levels. For example, rush hour peaks were obvious in these three regions on polluted days, and gradual growth was observed on excellent days. This means that the dPNC is likely determined by the total PNC rather than by the deposition fraction of particles. On the other hand, the dPNC in the ET and TB regions tended to be affected by NPF events, while the dPNC in the PUL region tended to be influenced by traffic emissions (Fig. 4).

Table S7 compares the daily deposited doses by particle number, mass, and surface area in the different airway regions. The D_{PNd} was dominated by UFPs (nucleation and Aitken modes), which accounted for 95%, 84%, and 78% of the total on excellent, good, and polluted days, respectively. On excellent days, the D_{PNd} was 94.0×10^9 particles day^{-1}, which was comparable with that on polluted days (~96.8×10^9 particles day^{-1}). However, the D_{PMd} increased linearly with the pollution level, as expected, because it was dominated by accumulation and coarse mode particles. Polluted days had the highest D_{PMd} (1071 μg day^{-1}), which was 6.4 times that on excellent days. The D_{PSd} was dominated by accumulation mode particles and polluted days had the highest D_{PSd} (282.3 cm^2 day^{-1}), which was 5.4 times that on

excellent days. These results suggest that the deposited doses based on particle mass and surface area concentrations are more sensitive to pollution levels than that based on particle number concentration and more attention should be paid to the exposure risk in terms of deposited number dose on excellent days.

3.5. Particle deposited dose based on different metrics in different regions of the respiratory tract

Fig. 5 compared the 24-h total deposited number, mass, and surface area dose in the respiratory tract of a Chinese adult, respectively. The D_{PNd} in the different airway regions decreased in the order PUL (~31.3×10^9 particles day^{-1}) > TB (~29.4×10^9 particles day^{-1}) > ET (~13.0×10^9 particles day^{-1}) (Fig. 5A). The D_{PNd} values in this study were lower than those reported in Italy, e.g., 65×10^9 particles day^{-1} in TB and 150×10^9 particles day^{-1} in PUL (Buonanno et al., 2011). Hussein et al. (2013) calculated the daily total D_{PNd} (3 – 950 nm) for an adult male from January to May 2009 in Helsinki. Their D_{PNd} were 40×10^9 particles day^{-1} on weekends and 57×10^9 particles day^{-1} on workdays, respectively. These values are lower than our results (80.4×10^9 particles day^{-1}) from 3 nm to 10 μm. The difference in the D_{PNd} should be ascribed to different pollution levels, the strength of NPF events and the size ranges of the measured particles in different environments.

As shown in Fig. 5B, more than half (60%, 202 μg day^{-1}) of the particle mass was deposited in the ET region. The sequence of D_{PMd} was ET > PUL > TB. This is consistent with that observed during the Diwali Festival in India (Izhar et al., 2018). A previous study (Varghese et al., 2005) reported the D_{PMd} of a women in Indian was 223.01 μg day^{-1} during cooking and 92.17 μg day^{-1} during non-cooking periods, respectivley, for particles with the $d_p < 3.1$ μm. These values were lower than our results (332 μg day^{-1}) due to the different exposure environments and the particle size ranges. In terms of deposited particle surface area, the total daily D_{PSd} was 97.2 cm^{-2} day^{-1} and 74% of the D_{PSd} was associated with accumulation mode particles (Fig. 5C).

Our results indicated that the majority of particles in terms of the number and surface area doses were deposited in the PUL region. This
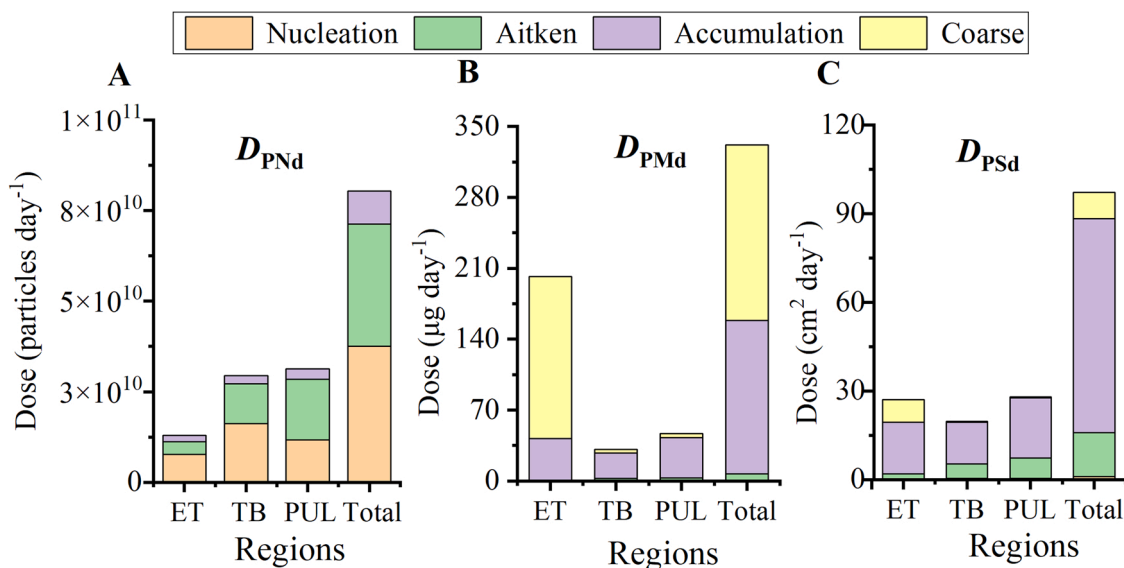
Fig. 5. Daily deposited particle dose. A. daily deposited number dose (D_{PNd}). B. daily deposited mass dose (D_{PMd}). C. daily deposited surface area dose (D_{PSd}) at different airway regions.

was different from that based on the mass dose, of which particles were preferentially deposited in the ET region. In addition, nucleation mode and Aitken mode particles dominantly contributed to the D_{PNd}, while coarse mode and accumulation mode particles were the main contributors to the D_{PMd} and D_{PSd}, respectively. Because fine particles are

usually treated as microorganisms by the immune system, the D_{PNd} might be more a reasonable indicator for connecting the potential risk from exposure to PM with TB and PUL disease than the D_{PMd}. UFPs are mainly generated from NPF, the combustion of transport fuels, and biofuel burning emissions. They are likely to carry toxic metals and
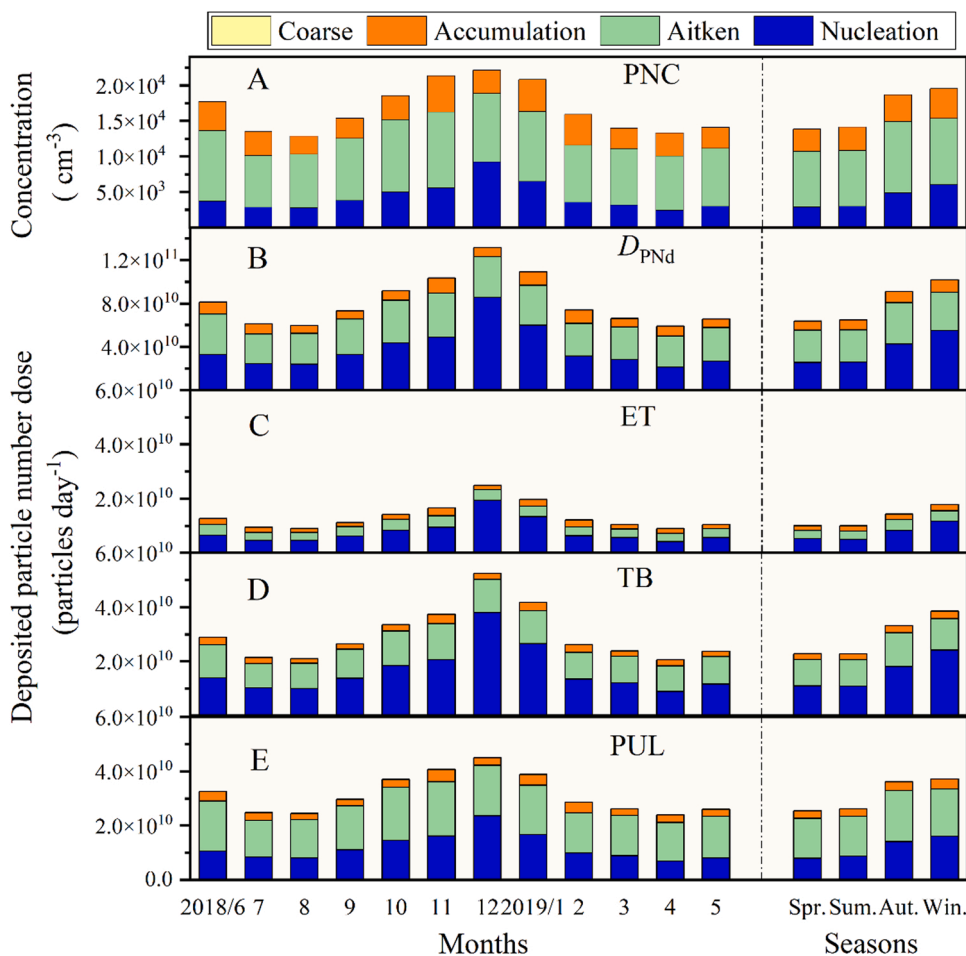

Fig. 6. Monthly and seasonal variations of particle number concentration (PNC) and deposited particle number dose (D_{PNd}) at different airway regions.

PAHs, subsequently, leading to impaired lung function, such as reduction in forced expiratory volume (FEV) and peak expiratory flow rate (PEFR), pulmonary inflammation, and finally increasing the risk of asthma and mortality in extreme cases (Kesavachandran et al., 2015). On the other hand, connections have been revealed between diseases such as pharyngitis and sinusitis and particles deposited in the ET region (Vincent, 2005). This means that number- or surface area-based particle concentrations are likely to be more sensitive health indicators for lower respiratory illness and/or cardiovascular diseases, while mass-based particle concentrations might be more sensitive to upper respiratory tract infection. These results suggest that different particle exposure metrics might provide useful indicators of the health risks of airborne particles. Thus, more attention should be given to the health effects of UFPs on the lower respiratory and cardiovascular systems in the future.

3.6. Temporal variations in particle deposition

The monthly and seasonal variations in the particle concentrations and daily D_{PNd}, D_{PMd}, and D_{PSd} in the different airway regions are shown in Fig. 6 and Fig S6- S7. The PNC values were highest in December (2.2×10^3 cm^{-3}) and lowest in August (1.3×10^3 cm^{-3}). The sequence of the PNC in different seasons was winter > autumn > summer > spring (Fig. 6A). Generally speaking, the deposited number dose (D_{PNd}) had similar monthly and seasonal variation with PNC (Fig. 6B). The contribution of Aitken mode particles to the D_{PNd} was relatively stable (~54%). However, the contribution of nucleation mode particles to the D_{PNd} showed obvious variation among the different months. The largest value was observed in December (42%), followed by January (31%), while it was approximately 22% in other months. The D_{PNd} in different seasons followed the order of: winter > autumn > summer > spring, corresponding with the seasonal NPF frequency, which was 46.6% (winter), 44.7% (autumn), 43.4% (spring), and 35.1% (summer) (Fig. S8). The NPF frequency in this study is generally consistent with recent work carried out in urban Beijing from 2018 to 2019 by Deng et al. (Deng et al., 2020). However, the NPF frequencies in June and August (35%) in this study were higher than those in previous studies in the same period of 2004–2007 (11–20%) (Wu et al., 2007, 2008) (26%) (Wang et al., 2011), and 2018 (16.7%) (Deng et al., 2020). The seasonal variations were less obvious for particles in other modes than for nucleation mode particles. It is noteworthy to note that nucleation mode particles contribute about 42~53% to the deposited dose in ET and TB regions while the PUL region is dominated by Aitken mode particles (53%) (Fig. 6B-D). Previous research showed nucleation mode particles mainly generated from local NPF events (Shen et al., 2016) and combustion sources. Traffic emissions have been considered to be the major source of Aitken mode particles in urban Beijing based on 2 years of observations (Wang et al., 2013). Our results showed that ET and TB-related impairments might be mostly associated with NPF events and combustion sources in winter, while PUL-related impairments might be more readily influenced by traffic sources regardless of the season in Beijing.

It should be noted that the total D_{PNd} in November was lower than that in December, although the PNC values in both months were comparable; meanwhile, the highest total D_{PNd} occurred in December, while the D_{PMd} (Fig. S7) and D_{PSd} (Fig. S8) were not so high. In addition, the D_{PMd} was very low in June and July due to the presence of fewer coarse particles, while the corresponding D_{PNd} and D_{PSd} were still relatively high. This can be explained by the fact that NPF events occurred frequently in December, June, and July, resulting in high concentrations of nucleation mode particles and subsequently contributing to the high D_{PNd}. This further highlights the role of NPF in the D_{PNd} in Beijing.

4. Conclusions and implications

NPF events occur mainly on days with excellent air quality, but their health effects have consistently been ignored. Based on one year of observations, we quantitatively evaluated the deposition potential of particles after accounting for hygroscopic growth in the human lung airways using the MPPD model. Our results highlighted the possible health effects of NPF events in Beijing. The D_{PNd} on excellent days was comparable to that on heavily polluted days due to the high frequency of NPF events (72.6%). However, the D_{PMd} on excellent days indicated the lowest exposure potential of all pollution levels. This implies that the risk of exposure to particles produced in NPF events is likely pretty high from the perspective of the particle number concentration but very low in terms of mass-based air quality standards.

The sequence of D_{PNd} in the respiratory tract was TB > PUL > ET on NPF days, while it was PUL > TB > ET on non-NPF days. The deposited particle number in nucleation mode, which accounted for 45% of the D_{PNd} in the TB region, on NPF days was 2 times great than that on non-NPF days. Our previous studies proposed that improvements in air quality can be achieved via reductions in gas-phase precursors of NPF, mainly dimethylamine, ammonia, and SO$_2$ (Kulmala et al., 2020). Additional benefits to human health, particularly for TB diseases, might be resulted from this kind of air pollution control strategy. However, a study showed that nucleation-mode particles, which have a large number concentration but contribute little to the surface area concentration, had a significant negative association with FeNO, a well-established biomarker of pulmonary inflammation (Gong et al., 2019). This means that NPF events might be associated with a high exposure risk in the TB region and more research is required on this topic in the future.

It should be pointed out that we investigated the deposition potential of inhaled particles based on ambient particle concentrations, which likely deviate from that in the actual exposure as people spend most of their time in room environments. In the future, the permeation efficiency of UPFs from outdoor to indoor environments should be determined to accurately evaluate the possible risk of exposure to UPFs.

CRediT authorship contribution statement

Li Ma: Methodology, analysis & writing - original draft. **Ying Zhang**: Investigation & analysis. **Zhuohui Lin**: Software & Analysis. **Ying Zhou**: Investigation. **Chao Yan**: Investigation & validation. **Yusheng Zhang**: Methodology & analysis. **Wenshuo Zhou**: Investigation & analysis. **Wei Ma**: Analysis. **Chenjie Hua**: Investigation & analysis. **Xiaoxiao Li**: Data curation & investigation. **Chenjuan Deng**: Data curation. **Yu Qi**: Analysis, review & editing. **Lubna Dada**: Methodology & analysis. **Hongyan Li**: Review & editing. **Federico Bianchi**: Review & editing. **Tuukka Petäjä**: Analysis, eview & editing. **Juha Kangasluoma**: Methodology, review & editing. **Jingkun Jiang**: Data curation, review & editing. **Sijin Liu**: Review & editing. **Tareq Hussein**: Methodology, review & editing. **Markku Kulmala**: Supervision, review & editing. **Yongchun Liu**: Methodology, analysis, supervision, review, editing, funding acquisition.

Declaration of Competing Interest

The authors declare that they have no known competing financial interests or personal relationships that could have appeared to influence the work reported in this paper.

Data availability

Data will be made available on request.

Acknowledgments

Appendix A. Supporting information

Supplementary data associated with this article can be found in the online version at doi:10.1016/j.ecoenv.2022.114023.

References

Almeida, A.S., Ferreira, R.M.P., Silva, A.M.S., Duarte, A.C., Neves, B.M., Duarte, R., 2020. Structural features and pro-inflammatory effects of water-soluble organic matter in inhalable fine urban air particles. Environ. Sci. Technol. 54, 1082–1091. https://doi.org/10.1021/acs.est.9b04596.

An, J., Wang, H., Shen, L., Zhu, B., Zou, J., Gao, J., et al., 2015. Characteristics of new particle formation events in Nanjing, China: effect of water-soluble ions. Atmos. Environ. 108, 32–40. https://doi.org/10.1016/j.atmosenv.2015.01.038.

Asgharian, B., 2004. A model of deposition of hygroscopic particles in the human lung. Aerosol Sci. Technol. 38, 938–947. https://doi.org/10.1080/027868290511236.

Buonanno, G., Giovinco, G., Morawska, L., Stabile, L., 2011. Tracheobronchial and alveolar dose of submicrometer particles for different population age groups in Italy. Atmos. Environ. 45, 6216–6224. https://doi.org/10.1016/j.atmosenv.2011.07.066.

Calderon-Garciduenas, L., Gonzalez-Maciel, A., Mukherjee, P.S., Reynoso-Robles, R., Perez-Guille, B., Gayosso-Chavez, C., et al., 2019. Combustion- and friction-derived magnetic air pollution nanoparticles in human hearts. Environ. Res. 176, 108567 https://doi.org/10.1016/j.envres.2019.108567.

Chalupa, D.C., et al., 2004. Ultrafine particle deposition in subjects with asthma. Environ. Health Perspect. 112 (8), 879–882. https://doi.org/10.1289/ehp.6851.

Chu, B., Dada, L., Liu, Y., Yao, L., Wang, Y., Du, W., et al., 2021. Particle growth with photochemical age from new particle formation to haze in the winter of Beijing, China. Sci. Total Environ. 753. https://doi.org/10.1016/j.scitotenv.2020.142207.

Cohen, A.J., Brauer, M., Burnett, R., Anderson, H.R., Frostad, J., Estep, K., et al., 2017. Estimates and 25-year trends of the global burden of disease attributable to ambient air pollution: an analysis of data from the global burden of diseases study 2015. Lancet 389, 1907–1918. https://doi.org/10.1016/s0140-6736(17)30505-6.

Daigle, C.C., David, C.C., Gibb, F.R., Morrow, P.E., Oberdörster, G., Frampton, M.W., et al., 2003. Ultrafine particle deposition in humans during rest and exercise. Inhal. Toxicol. 15 (6), 539–552. https://doi.org/10.1080/08958370304468.

Deng, C., Fu, Y., Dada, L., Yan, C., Cai, R., Yang, D., et al., 2020. Seasonal characteristics of new particle formation and growth in urban Beijing. Environ. Sci. Technol. 54, 8547–8557. https://doi.org/10.1021/acs.est.0c00808.

Donaldson, K., Brown, D., Clouter, A., Duffin, R., Macnee, W., Renwick, L., et al., 2002. The pulmonary toxicology of ultrafine particles. J. Aerosol Med. 15, 213–220. https://doi.org/10.1089/089426802320282338.

Gao, J., Chai, F., Wang, T., Wang, S., Wang, W., 2012. Particle number size distribution and new particle formation: New characteristics during the special pollution control period in Beijing. J. Environ. Sci. 24, 14–21. https://doi.org/10.1016/s1001-0742 (11)60725-0.

Gong, J., Zhu, T., Hu, M., Wu, Z., Zhang, J.J., 2019. Different metrics (number, surface area, and volume concentration) of urban particles with varying sizes in relation to fractional exhaled nitric oxide (FeNO). J. Thorac. Dis. 11 (4), 1714. https://doi.org/10.21037/jtd.2019.03.90.

Hu, M., Peng, J., Sun, K., Yue, D., Guo, S., Wu, Z., et al., 2012. Estimation of size-resolved ambient particle density based on the measurement of aerosol number, mass, and chemical size distributions in the winter in Beijing. Environ. Sci. Technol. 46 (18), 9941–9947. https://doi.org/10.1021/es204073t.

Hussein, T., Londahl, J., Paasonen, P., Koivisto, A.J., Petaja, T., Hameri, K., et al., 2013. Modeling regional deposited dose of submicron aerosol particles. Sci. Total Environ. 458–460, 140–149. https://doi.org/10.1016/j.scitotenv.2013.04.022. PMID: 23644567.

Izhar, S., Rajput, P., Gupta, T., 2018. Variation of particle number and mass concentration and associated mass deposition during Diwali festival. Urban Clim. 24, 1027–1036. https://doi.org/10.1016/j.uclim.2017.12.005.

Ji, D., Zhang, J., He, J., Wang, X., Pang, B., Liu, Z., et al., 2016. Characteristics of atmospheric organic and elemental carbon aerosols in urban Beijing, China. Atmos. Environ. 125, 293–306. https://doi.org/10.1016/j.atmosenv.2015.11.020.

Kesavachandran, C.N., Kamal, R., Bihari, V., Pathak, M.K., Singh, A., 2015. Particulate matter in ambient air and its association with alterations in lung functions and respiratory health problems among outdoor exercisers in national capital region, India. Atmos. Pollut. Res. 6, 618–625. https://doi.org/10.5094/apr.2015.070.

Kulmala, M., Dada, L., Dllenbach, K., Yan, C., Kerminen, V-M., et al., 2020. Is reducing new particle formation a plausible solution to mitigate particulate air pollution in Beijing and other Chinese megacities? Faraday Discuss. 226, 334–347. https://doi.org/10.1039/D0FD00078G.

Li, S., Zou, B., You, J., Fang, X., Zhao, X., Yao, X., 2018. Satellite-based china's PM2.5 pollution and associated premature mortality measurement over past two decades. Remote Sens. Spat. Inf. Sci. XLII-3/W5, 39–45. https://doi.org/10.5194/ISPRS-ARCHIVES-XLII-3-W5-39-2018.

Li, X., Yan, C., Patterson, R.F., Zhu, Y., Yao, X., Zhu, Y., et al., 2016. Modeled deposition of fine particles in human airway in Beijing, China. Atmos. Environ. 124, 387–395. https://doi.org/10.1016/j.atmosenv.2015.06.045.

Liu, Y., Yan, C., Feng, Z., Zheng, F., Fan, X., Zhang, Y., et al., 2020. Continuous and comprehensive atmospheric observations in Beijing: a station to understand the complex urban atmospheric environment. Big Earth Data 4, 295–321. https://doi.org/10.1080/20964471.2020.1798707.

Liu, Z., Hu, B., Ji, D., Wang, Y., Wang, M., Wang, Y., 2015. Diurnal and seasonal variation of the PM2.5 apparent particle density in Beijing, China. Atmos. Environ. 120, 328–338. https://doi.org/10.1016/j.atmosenv.2015.09.005.

Lu, D., Luo, Q., Chen, R., Zhuansun, Y., Jiang, J., Wang, W., et al., 2020. Chemical multi-fingerprinting of exogenous ultrafine particles in human serum and pleural effusion. Nat. Commun. 11, 2567. https://doi.org/10.1038/s41467-020-16427-x.

Manojkumar, N., Srimuruganandam, B., Shiva Nagendra, S.M., 2019. Application of multiple-path particle dosimetry model for quantifying age specified deposition of particulate matter in human airway. Ecotoxicol. Environ. Saf. 168, 241–248. https://doi.org/10.1016/j.ecoenv.2018.10.091.

Maso, M.D., Kulmala, M., Riipinen, I., Wagner, R., Hussein, T., Aalto, P.P., et al., 2005. Formation and growth of fresh atmospheric aerosols: eight years of aerosol size distribution data from SMEAR II, Hyytiala, Finland. Boreal Environ. Res. 10, 323–336.

Massling, A., Stock, M., Wehner, B., Wu, Z.J., Hu, M., Brueggemann, E., et al., 2009. Size segregated water uptake of the urban submicrometer aerosol in Beijing. Atmos. Environ. 43, 1578–1589. https://doi.org/10.1016/j.atmosenv.2008.06.003.

Miller, M.R., Raftis, J.B., Langrish, J.P., McLean, S.G., Samutrtai, P., Connell, S.P., et al., 2017. Inhaled nanoparticles accumulate at sites of vascular disease. ACS Nano 11, 4542–4552. https://doi.org/10.1021/acsnano.6b08551.

Morawska, L., Keogh, D.U., Thomas, S.B., Mengersen, K., 2008. Modality in ambient particle size distributions and its potential as a basis for developing air quality regulation. Atmos. Environ. 42, 1617–1628. https://doi.org/10.1016/j.atmosenv.2007.09.076.

Oberdorster, G., Sharp, Z., Atudorei, V., Elder, A., Gelein, R., Kreyling, W., et al., 2004. Translocation of inhaled ultrafine particles to the brain. Inhal. Toxicol. 16, 437–445. https://doi.org/10.1080/08958370490439597.

Paital, B., Agrawal, P.K., 2021. Air pollution by NO2 and PM2.5 explains covid-19 infection severity by overexpression of angiotensin-converting enzyme 2 in respiratory cells: a review. Environ. Chem. Lett. 19, 25–42. https://doi.org/10.1007/s10311-020-01091-w. PMID:32982622.

Park, K., Park, J.Y., Kwak, J.-H., Cho, G.N., Kim, J.-S., 2008. Seasonal and diurnal variations of ultrafine particle concentration in urban Gwangju, Korea: observation of ultrafine particle events. Atmos. Environ. 42, 788–799. https://doi.org/10.1016/j.atmosenv.2007.09.068.

Roy, M., Becquemin, M.H., Bouchikhi, A., 1991. Ventilation rates and lung volumes for lung modelling purposes in ethnic groups. Radiat.Prot. Dosim. 38, 49–55. https://doi.org/10.1093/rpd/38.1–3.49.

Shen, X.J., Sun, J.Y., Zhang, X.Y., Zhang, Y.M., Zhang, L., Fan, R.X., et al., 2016. The influence of emission control on particle number size distribution and new particle formation during China's V-day parade in 2015. Sci. Total Environ. 573, 409–419. https://doi.org/10.1016/j.scitotenv.2016.08.085.

Sioutas, C., Delfino, R.J., Singh, M., 2005. Exposure assessment for atmospheric ultrafine particles (UFPs) and implications in epidemiologic research. Environ. Health Perspect. 113, 947–955. https://doi.org/10.1289/ehp.7939.

Sjogren, S., Gysel, M., Weingartner, E., Baltensperger, U., Cubison, M.J., Coe, H., et al., 2007. Hygroscopic growth and water uptake kinetics of two-phase aerosol particles consisting of ammonium sulfate, adipic and humic acid mixtures. Aerosol Sci. 38, 157–171. https://doi.org/10.1016/j.jaerosci.2006.11.005.

Terzano, C., Di Stefano, F., Conti, V., Graziani, E., Petroianni, A., 2010. Air pollution ultrafine particles: toxicity beyond the lung. Eur. Rev. Med. Pharmacol. Sci. 14, 809–821. https://doi.org/10.1016/j.euroneuro.2010.05.003.

Tie, X.X., Wu, D., Brasseur, G., 2009. Lung cancer mortality and exposure to atmospheric aerosol particles in Guangzhou, China. Atmos. Environ. 43, 2375–2377. https://doi.org/10.1016/j.atmosenv.2009.01.036.

Vincent, James H., 2005. Health-related aerosol measurement: a review of existing sampling criteria and proposals for new ones. J. Environ. Monit. 7, 1037–1053. https://doi.org/10.1039/b509617k.

Vu, T.V., Delgado-Saborit, J.M., Harrison, R.M., 2015. A review of hygroscopic growth factors of submicron aerosols from different sources and its implication for calculation of lung deposition efficiency of ambient aerosols. Air Qual. Atmos. Health 8, 429–440. https://doi.org/10.1007/s11869-015-0365-0.

Wagner, P., Schäfer, K., 2017. Influence of mixing layer height on air pollutant concentrations in an urban street canyon. Urban Clim. 22, 64–79. https://doi.org/10.1016/j.uclim.2015.11.001.

Wang, Z.B., Hu, M., Yue, D.L., Zheng, J., Zhang, R.Y., Wiedensohler, A., et al., 2011. Evaluation on the role of sulfuric acid in the mechanisms of new particle formation for Beijing case. Atmos. Chem. Phys. 11, 24165–24189. https://doi.org/10.5194/acp-11-24165-2011.

Wang, Z.B., Hu, M., Wu, Z.J., Yue, D.L., He, L.Y., Huang, X.F., et al., 2013. Long-term measurements of particle number size distributions and the relationships with air mass history and source apportionment in the summer of Beijing. Atmos. Chem. Phys. 13, 5165–5197. https://doi.org/10.5194/acp-13-5165-2013.

Wu, Z., Hu, M., Liu, S., Wehner, B., Bauer, S., Ma ßling, A., et al., 2007. New particle formation in Beijing, China: statistical analysis of a 1-year data set. J. Geophys. Res 112. https://doi.org/10.1029/2006jd007406.

Wu, Z., Hu, M., Lin, P., Liu, S., Wehner, B., Wiedensohler, A., 2008. Particle number size distribution in the urban atmosphere of Beijing, China. Atmos. Environ. 42, 7967–7980. https://doi.org/10.1016/j.atmosenv.2008.06.022.

Zhang, Q., Zheng, Y., Tong, D., Shao, M., Wang, S., Zhang, Y., et al., 2019. Drivers of improved PM2.5 air quality in China from 2013 to 2017. Proc. Natl. Acad. Sci. USA 116, 24463–24469. https://doi.org/10.1073/pnas.1907956116.

Zhou, Y., Dada, L., Liu, Y., Fu, Y., Kangasluoma, J., Chan, T., et al., 2020. Variation of size-segregated particle number concentrations in wintertime Beijing. Atmos. Chem. Phys. 20, 1201–1216. https://doi.org/10.5194/acp-20-1201-2020.